Available online at www.sciencedirect.com
ScienceDirect
Remote Sensing of Environment 106 (2007) 326–336
Remote Sensing of Environment
www.elsevier.com/locate/rse

Near-real time retrievals of land surface temperature within the MODIS Rapid Response System

A.C.T. Pinheiro [a,b,*], J. Descloitres [c], J.L. Privette [b], J. Susskind [a], L. Iredell [d], J. Schmaltz [c]

[a] NASA Goddard Space Flight Center, Greenbelt, MD, USA
[b] NOAA National Climatic Data Center, Asheville, NC, USA
[c] Science Systems and Applications, Inc. (SSAI), NASA GSFC, Greenbelt, MD, USA
[d] Science Applications International Corporation (SAIC), NASA GSFC, Greenbelt, MD, USA

Received 4 October 2005; received in revised form 31 August 2006; accepted 3 September 2006

Abstract

The MODIS Rapid Response (RR) System was developed to meet the near real time needs of the applications community. Generally, its products are available online within hours of the satellite overpass. We recently adapted the standard MODIS land surface temperature (LST) split-window algorithm for use in the RR System. To minimize latency, we eliminated the algorithm's dependency on upstream MODIS products. For example, although the standard MODIS LST requires prior retrieval of air temperature and water vapor from the MODIS scene, the RR LST employs a climatological database of atmospheric values based on a 25-year record of NOAA TOVS observations. The standard and RR algorithms also differ in upstream processing, surface emissivity determination, and use of a cloud mask (RR product does not contain one). Comparison of the MODIS RR and standard LST products suggests that biases are generally less than 0.1 K, and root-mean-square differences are less than 1 K despite the presence of some larger outliers. Initial validation with field data suggests the absolute uncertainty of the RR product is below 1 K. The MODIS RR land surface temperature algorithm is a stand-alone computer code. It has no dependencies on external products or toolkits, and is suitable for Direct Broadcast and other processing systems.

Keywords: Land surface temperature; MODIS; Rapid Response System; Direct broadcast

1. Introduction

Through the first 2 years of Terra satellite operations, the Earth Observing System (EOS) Data Information System (DIS) – designed for processing, distributing and archiving EOS data – suffered various problems that limited product generation rates. In that period, product generation lagged data acquisition by up to 2 months. To address the needs of applications user communities – especially the U.S. Forest Service in their efforts to combat the devastating wildfires of 2000 – the MODIS Land Discipline Team developed the Rapid Response (RR) System at NASA's Goddard Space Flight Center, in collaboration with the University of Maryland. Initial emphasis was on delivering MODIS corrected reflectance and active fire products within 2 to 4 h of acquisition (Justice et al., 2002).

The initial RR project successes, coupled with early challenges in producing and using standard MODIS products (e.g., uncommon projections and data formats, extensive metadata and quality assurance information, up to 50 days latency), led to RR product requests from other users. The RR mission thus evolved into developing and distributing modified MODIS land products within hours of the satellite observation, at accuracies rivaling the standard products and catered to the needs (e.g., data products, projections, formats, content, subsets) of (primarily) application-oriented users. The project's flexibility (e.g., subsetting, multiple projections) facilitates production of custom products for high volume data users that are not available via standard MODIS processing.

Although current latency for standard MODIS products is typically less than 2 days, operational, emergency and media communities, such as the U.S. Forest Service, the National

* Corresponding author. NASA Goddard Space Flight Center, Greenbelt, MD, USA. Tel.: +1 828 271 4453; fax: +1 828 271 4328.
E-mail addresses: Ana.Pinheiro@noaa.gov, Ana.Pinheiro@gsfc.nasa.gov

0034-4257/$ - see front matter © 2006 Elsevier Inc. All rights reserved.
doi:10.1016/j.rse.2006.09.006

Interagency Fire Center (NIFC) and the U.N. Global Fire Monitoring Center, continue to rely extensively on RR system's capabilities. Through early 2004, the RR product suite consisted of active fire distribution, Normalized Difference Vegetation Index (NDVI) and atmospherically-corrected reflectance imagery and products.

Recently, we developed and implemented a land surface temperature (LST) product within the RR system. Our algorithm was adapted from that of the MODIS Level 2 "swath" product (MOD11_L2 for Terra, MYD11_L2 for Aqua), hereafter referred to as the standard LST product. The RR LST algorithm provides day and night products at 1-km spatial resolutions globally in swath format. LST is a key variable needed to describe the energetic state of the Earth's surface, and its availability in near real time can benefit various hydrological, ecological, and biogeochemical applications.

The objective of this paper is to describe the implementation the LST product within the MODIS RR System and to detail the changes in the standard algorithm as required for near-real time production. We first introduce the MODIS sensor and the standard MODIS LST product. Then we describe the MODIS RR System, focusing on the LST algorithm. We explain the assumptions inherent to our approach and describe the TOVS climatology input field. We evaluate the RR product against the standard product and field measurements. Finally, we present a discussion and conclusions.

2. Background

2.1. Moderated Resolution Imaging Spectroradiometer (MODIS) sensor

The Moderated Resolution Imaging Spectroradiometer (MODIS) is an Earth Observing System (EOS) instrument on board the Terra and Aqua platforms, launched in December 1999 and May 2002, respectively. The sensor scans ±55° from nadir in 36 spectral bands. During each scan, 10 along-track detectors per spectral band simultaneously sample the earth. From its polar orbit, MODIS provides daytime and nighttime global coverage every 1 to 2 days.

MODIS has 16 bands in the emissive portion (3–15 μm) of the spectrum. The bands have a ground instantaneous field of view of about 1 km at nadir and a radiometric resolution of 12 bits. The detectors sample onboard calibration before and after each scan of the Earth (Guenther et al., 2002). The absolute calibration accuracy is within 1% for the thermal infrared bands, except for band 36 (Justice et al., 2002). In this article, we focus on the two longwave thermal infrared bands, 31 and 32, used in the split-window LST retrieval. Mean band characteristics are provided in Table 1.

Table 1
MODIS emissive bands for surface temperature retrievals

Band	Band width (μm)	Central wavelength (μm)	Required NeΔT (K)
31	10.780 – 11.280	11.0186	0.05
32	11.77 – 12.27	12.0325	0.05

2.2. MODIS land surface temperature swath product

The standard MODIS LST product suite is composed of both swath products, which cover areas sampled by MODIS in a 5-min period (about 2030 km along-track, and 2330 km cross-track), and gridded 'tile' products (about 10° × 10° at the equator), which are typically composed of data from multiple swaths and amenable to compositing and aggregation.

The MODIS standard LST product is generated using a generalized split-window algorithm, which is derived from a (typically) 1st order Taylor Series expansion of the radiative transfer equation. The coefficients for the algorithm are determined through regression analysis of radiative transfer simulations (prescribed LSTs vs. simulated top-of-atmosphere brightness temperatures) for a wide range of surface and atmospheric conditions. The split window method uses two spectrally-close bands in the thermal infrared wavelengths, and assumes that the differential radiance between these bands is a linear function of the atmospheric absorption at those wavelengths (due primarily to water vapor). However, to estimate the kinetic (skin) temperature, surface emissivity values are typically required for one or more terms in a split window formulation. Surface emissivity is the ratio of the radiation emitted by an object at a given temperature to the radiation emitted by a backbody (perfect emitter) at the same temperature and in the same spectral wavelength.

The split window used for MODIS was developed by Wan and Dozier (1996), and is defined as,

$$T_s = C + \left(A_1 + A_2\frac{1-\varepsilon}{\varepsilon} + A_3\frac{\Delta\varepsilon}{\varepsilon^2}\right)\frac{T_{31}+T_{32}}{2} + \left(B_1 + B_2\frac{1-\varepsilon}{\varepsilon} + B_3\frac{\Delta\varepsilon}{\varepsilon^2}\right)\frac{T_{31}-T_{32}}{2} \quad (1)$$

where T_{31} and T_{32} are the brightness temperatures measured in the MODIS bands 31 and 32, respectively; and A_1, A_2, A_3, B_1, B_2, B_3 and C are regression coefficients. These coefficients are available during algorithm execution via a look up table (LUT) stratified by subranges of near surface air temperature and total column water vapor. These input fields are obtained at 5 km × 5 km resolution from the MOD07_L2 product.

The emissivity values in Eq. (1) are obtained based on a landcover classification approach. The algorithm determines each pixel's land cover class from MODIS gridded land cover product (MOD12Q1). The MODIS land processing system's Collection 4 (v004) LST algorithm uses a landcover derived from Collection 3 (v003) data collected between 2001 and 2002.

Once the landcover type for a given pixel is identified, the emissivities ε_{31} and ε_{32} are retrieved from a LUT. For pixels in which MODIS angle of observation is above 42.3° (0.73827 rad), an adjustment to the emissivity is used to account for directional emissivity variation following Eqs. (2) and (3).

$$\varepsilon_{31} = \varepsilon_{31} + \text{ang\_}\varepsilon_{31} * (\theta_v - 0.73827) \quad (2)$$

$$\varepsilon_{32} = \varepsilon_{32} + \text{ang\_}\varepsilon_{32} * (\theta_v - 0.73827), \quad (3)$$

where θ_v is expressed in radians. Coefficients ang_ε_{31} and ang_ε_{32} are retrieved also from a LUT. The emissivity values are then calculated as follows:

$$\varepsilon = \frac{\varepsilon_{31} + \varepsilon_{32}}{2} \tag{4}$$

$$\Delta\varepsilon = \varepsilon_{31} - \varepsilon_{32}. \tag{5}$$

The standard LST product is produced at 1 km spatial resolution for each MODIS scene acquired. LST values are estimated only for pixels associated with clear-sky conditions, identified by the MODIS cloud mask (MOD35_L2) at 99% confidence for land surfaces, and 66% confidence for inland water bodies. A fill value is used for other pixels. In addition to the LST field, a swath LST product file contains several other data layers that include quality control (QC) flags, the estimated error in LST, the surface emissivity used for bands 31 and 32, the view zenith angle, the view time, and the latitude and longitude. The product is archived in the Land Processes Data Active Archive Center (LP DAAC).

3. MODIS Rapid Response System

The MODIS RR System is designed to provide MODIS land products to the user community as quickly as possible. Algorithm efficiencies are achieved in part by eliminating external dependencies such as the assimilated climate and post-processed geolocation data used by the core MODIS processing system (Sohlberg et al., 2001).

3.1. MODIS Rapid Response land surface temperature

The RR LST algorithm is adapted from the standard algorithm, but with several changes designed to facilitate near-real time processing. Below we describe these changes.

3.1.1. Radiometric calibration of emissive bands

In both the standard and RR LST algorithms, the MODIS Level-1B radiance data (MOD021KM) for bands 31 and 32 are calibrated using the radiance-scales and offsets provided with each MODIS granule. The radiance (L) values are then converted to brightness temperature (Tb) using the inverse of the Plank function (Eq. (6)):

$$\mathrm{Tb} = \frac{c_2/\lambda}{\ln\left(1 + \frac{c_1}{L^*\lambda^5}\right)} \tag{6}$$

with c1 = 1.19107×10^8 W μm^4 m^{2}sr, and c2 = 1.43883×10^4 μm K, for center wavelength of the given band (31 or 32). For the standard algorithm, Eq. (6) is determined by convolving it with the average detector spectral response function (weighted integration method) for each of the two thermal bands. The results are stored in a LUT to decrease the computational time during operation. However, given the small temperature increments within the LUT, its size is quite large.

In our RR implementation, we sought to avoid the computational expense needed to load and parse through the LUT. We therefore evaluate Eq. (6) directly using an adaptation of the 'center wavelength method', where the equation is determined at a single representative wavelength rather than through convolution with a response function. In our adaptation, we optimally adjusted the single wavelength to that producing the minimum difference in Tb from the weighted integration method. Because each of the 10 along-track detectors has a slightly different response function, we determined the optimal wavelength for each detector individually.

The use of the single wavelength approach in evaluating Eq. (6) introduces some error in Tb (see solid lines in, e.g., Fig. 1). Near the saturation temperatures of the respective bands (Terra platform: 392 K for band 31 and 340 K for band 32; Aqua: 387 K for band 31 and 340 K for band 32), these errors can exceed 0.1 K (e.g., 0.143 for band 31, detectors 8, 9 and 10 on Terra). To reduce these errors, we adapted a method first used in the MODIS RR fire product, where a linear correction is applied to each channel following Eq. (7):

$$\mathrm{Tb\_corrected} = \mathrm{Tb\_uncorrected}^*\mathrm{slope} + \mathrm{offset} \tag{7}$$

where Tb_uncorrected represents the value estimated in Eq. (6) using a single-wavelength. The slope and offset values were determined by regressing Tb values determined with the wavelength integration method against Tb_uncorrected values. Differences between the corrected and uncorrected Tb values are negligible (see dashed lines in Fig. 1), and well below the noise-equivalent delta temperatures (NEDT; see Table 1) for the bands.

3.1.2. Provision of atmospheric data sets

In the standard algorithm, coefficients for Eq. (1) are stratified by subranges of near surface air temperature and total column water vapor. During processing, these atmospheric values are determined from the MODIS product (MOD07_L2). The time required to generate MOD07_L2 unavoidably leads to greater latency in the standard LST product.

In the RR system, to avoid the time needed to generate the atmospheric parameters, we used a monthly climatology of near-surface air temperature (K) and total water column water vapor (cm) determined from the TIROS (Television Infrared Observation Satellite) Operational Vertical Sounder (TOVS) (Susskind et al., 1997). This choice follows our sensitivity study which showed that LST from Eq. (1) is not highly sensitive to errors in the input values of water vapor and surface air temperature.

The TOVS climatology is based on the monthly mean values of 25 years (1979–2003) of TOVS soundings. The water vapor and surface temperature values were adjusted to the average local equator crossing time of Terra (10:30 AM and PM) and Aqua (1:30 AM and PM) satellites. The adjustment, described in detail in Appendix A, uses a Fourier expansion of the time dependence of retrieved geophysical parameters in terms of both local time and time of year, with coefficients determined as a function of geographical location. For each geographical location, diurnal differences of the 23 years of the set of monthly mean retrieved parameters are used to generate coefficients. The coefficients were determined using observations made at the two to four

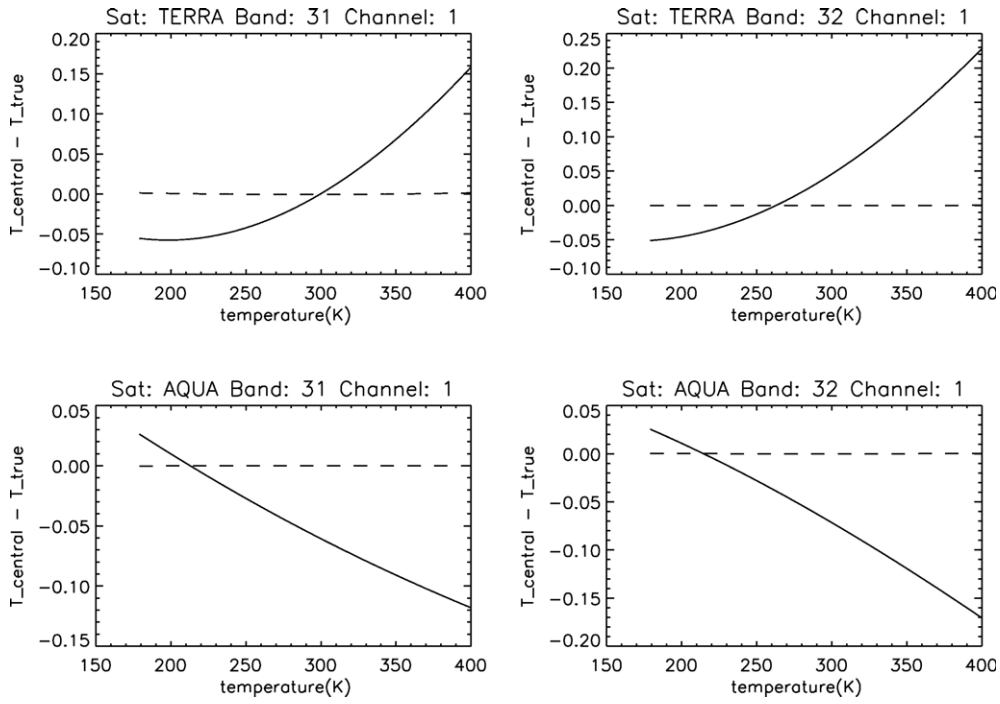

Fig. 1. Error in brightness temperature (Tb) retrievals using the single-wavelength approach before (solid line) and after (dashed line) application of the linear correction (Eq. (7)). Results for other detectors were similar.

different local crossing times observed by the one or two satellites operational in that month. These results were smoothed and projected onto a 1°×1° latitude–longitude grid (360×180 values) separately for Terra and Aqua.

During RR processing, the atmospheric parameters are estimated by interpolating the TOVS monthly mean values in time using a linear interpolation, and interpolated in space using bilinear interpolation. The results are used to determine the appropriate coefficient set for Eq. (1). Note that this approach is self-contained and that external data feeds are not required.

3.1.3. Estimation of target emissivity

Following the standard algorithm, the emissivity values for bands 31 and 32 in the RR algorithm are estimated based on the landcover classification. In the standard algorithm, the emissivity values are found by loading the requisite set of 10°×10° MODIS land cover tiles that overlap sections of the swath. To reduce the computation expense of loading several tiles for each swath, the RR system loads the relevant latitudinal belt of a global land cover map. This global map is in the Plate Carrée projection (Binary MOD12Q1 1 km Land Cover), and is available directly from the MODIS land cover developers (http://duckwater.bu.edu/lc/mod12q1.html). The RR algorithm uses the same IGBP land cover classification scheme as does the MOD11_L2 algorithm. The RR algorithm uses a nearest neighbor approach to choose the grid cell within the land cover product.

3.1.4. Rapid Response LST product

The RR LST product is generated for each granule acquired by MODIS Terra and MODIS Aqua. Three science data sets comprise each HDF4.1 product file: brightness temperature in channel 31, brightness temperature in channel 32, and LST. The RR LST imagery is available daily at the MODIS Rapid Response System web page (http://rapidfire.sci.gsfc.nasa.gov/) in JPEG format.

Note that no cloud screening is used in the RR algorithm. This decision follows feedback from some users of the standard MODIS LST product who believe that cloud filtering in that product removes useful thermal information. Our approach is also consistent with other RR products. As a result, the RR LST field is spatially continuous, whereas the standard product contains fill values where clouds are detected. Depending on the application, this may or may not be desirable. Other differences between the two products are identified in Table 2.

Fig. 2a illustrates an example of the MOD11_RR product for a granule retrieved by MODIS Aqua over north-east Africa and the Red Sea on January 1st 2003. It is easy to distinguish the cooler water surfaces of the Red Sea, in the range of 290s K contrasting with the land surfaces at higher temperatures, mostly above 300 K. Note that in the top-left and bottom-right portions of the granule, cloud contamination is visible in both LST image (Fig. 2a) as in the true color (Fig. 2c) image.

4. Evaluation of the Rapid Response LST product

We evaluated the RR product by comparing it to both the standard product and to field data. This comparison was performed for different atmospheric conditions (near-surface air temperature and water vapor) and at different latitudes and longitudes. The MODIS standard LST products used in our analysis are from reprocessing Collection 4.

Table 2
Main characteristics of Rapid Response and standard LST products

Characteristic	Standard LST	Rapid Response LST
Theoretical basis	Wan and Dozier (1996)	Wan and Dozier (1996)
Atmospheric water vapor	MOD07_L2*	TOVS climatology
Near-surface air temperature	MOD07_L2	TOVS climatology
Landcover (LC)	MOD12Q1	Binary MOD12Q1
Projection	Sinusoidal	Plate Carree
Spatial Resolution	0.08333° × 0.08333°	0.08333° × 0.08333°
Format	10° × 10° tiles, HDF-EOS	Global file, binary
Latency	<2 days	~3 h
Product format	HDF-EOS	HDF4.1
Cloud screening	Yes (MOD35_L2)	No

* A guide to the official MODIS products is available at http://modis-atmos.gsfc.nasa.gov.

4.1. Comparison with the standard LST product

We assessed the bias (mean difference) between the products, the precision (standard deviation) and the uncertainty (root mean square error) of the RR product globally for two dates: 1 January 2003 and 1 July 2003. These dates likely span earth's atmosphere/climate range for both the northern and southern hemispheres. The standard product was used as the true or reference temperature in the comparison. Note that although we are using global land observations, the dominance of land in the northern hemisphere significantly biases the analysis towards the dominant season in the northern latitudes.

All MODIS granules (daytime and nighttime) acquired on these dates were included in the evaluation. However, we selected for the comparison only land pixels (landmask = 1) and cloud free pixels (as defined in the standard product). A total of 483 granules and approximately 200 million pixels were therefore considered.

4.1.1. Results

We stratified our results for all granules and for day and night granules separately as shown in Table 3. The 'Total # pixels' reflect the sum of the 'Day' and 'Night' plus the granules classified as 'Both' (for retrieval conditions near solar terminator).

Results suggest that the two products agree well. The bias observed for daytime and nighttime retrievals tend to have opposite signs, suggesting that the RR product underestimates the standard product for daytime observations and overestimates the signals for nighttime observations. The global statistics (indicated in Table 3 as 'All') suggest the RR LST tends to overestimate, although the biases observed are always <0.1 K. For both dates, the product differences are lowest for daytime data (in bias, precision and uncertainty). In general, differences between the standard and the RR products increase for increasing values of LST.

Further analysis suggests that the product differences vary latitudinally. Specifically, the RR LST can differ substantially (up to 2 K) from the standard product at low latitudes (±20°) in both July and January. In January, the errors decrease steadily toward the South Pole (summer; <0.25 K over Antarctica). To the north, errors decrease in the mid latitudes (<0.25 K) before increasing slightly (0.25–0.5 K) at highest latitudes (polar winter). In July, the errors decrease (<0.25 K) to the south

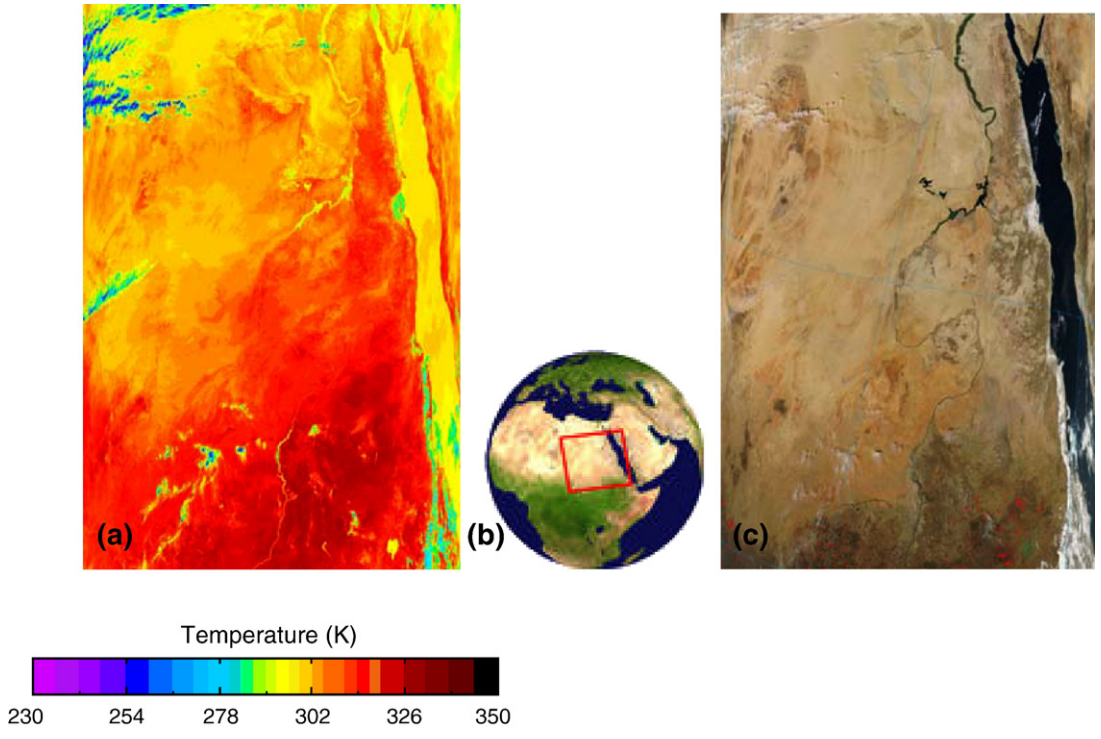

Fig. 2. MODIS Rapid Response a) land surface temperature b) RR granule location, and c) true color observation of north-east Africa and the Red Sea. Observation made by MODIS Aqua on 1 January 2003, at 11:15 UTC.

Table 3
Statistical comparison of MOD11_L2 and MOD11_RR, for MODIS-Aqua

	Accuracy (K) (bias)	Precision (K) (S.D.)	Uncertainty (K) (RMSE)	No. of pixels (N)	No. of granules (N)
1 January 2003					
All	0.014	0.464	0.554	110, 430,000	239
Day	−0.074	0.357	0.429	56,640,400	101
Night	0.093	0.666	0.799	39,113,340	108
1 July 2003					
All	0.081	0.707	0.935	87,708,800	244
Day	−0.189	0.646	0.779	38,967,300	114
Night	0.362	0.771	1.097	42,280,400	106

before increasing significantly (1–2 K) over the Antarctic ice sheet. To the north (polar summer), the errors are low in both mid and high latitudes (<0.25 K).

An example of the spatial distribution of LST errors (against the standard product) is provided in Fig. 3 for a scene acquired on January 1st 2003 at 11:15 AM UTC. The scene covers the same area shown in Fig. 2. The pixels depicted in black (about 50% of the entire granule) correspond to conditions identified as cloudy by the standard product, or classified as non-land. The dominant range of colors in Fig. 3 are white, corresponding to errors of ±0.25 K, and green tones, corresponding to errors <1 K. Note that the horizontal stripes in the left (upper and center) portions of the image are due to gaps in the standard product resulting from excessive noise in one channel of MODIS band 22, an input to the MODIS standard cloud algorithm. This discontinuity is propagated to the standard LST product. As shown in Fig. 2a this striping is not present in the RR LST product since no cloud screening is used by this algorithm.

Fig. 3. LST error spatial distribution for granule collected on January 1st, 2003 at 11:15 AM UTC.

A histogram of differences is shown in Fig. 4 for the same granule as above. Errors in the RR product were defined as the difference between it and the standard product. About 1.4 million pixels were classified as both land and non-cloudy and hence were used for this analysis. The mean bias was 0.35 K and the standard deviation (precision) was 0.46 K. The uncertainty was 0.58 K, slightly above the mean values found for all global daytime observations (0.43 K; see Table 3). The histogram shows a pseudo-bimodal curve, with the two peaks straddling 0 K. Within the full scene, the maximum difference was 4.8 K — clearly an outlier according to the histogram representation.

4.2. Validation with field measurements

The comparisons above indicate that, with respect to the standard product, the RR product is robust, has minimal bias, and behaves reasonably over the global distribution of land covers and atmospheric conditions. However, comparisons with high quality field measurements are required to assess absolute product uncertainty. We therefore compared the RR product to two sets of published field data used to validate the standard product.

The first data set was collected by Wan et al. (2002) over inland lakes, grasslands, rice cropland and snow covered areas on 10 dates in years 2000 and 2001 (see Table 4 for precise locations, land covers and times). The sites were chosen to be fairly homogeneous at the scale of MODIS measurements. The reported values represent the mean of multiple calibrated field radiometers. In addition, radiosondes were used to measure the column water vapor. The second data set was measured by Coll et al. (2005) over two sites in Spain (see Table 5 for precise locations and times). The first site was sampled on seven dates in July/August 2002 and 2003, and the second site was measured on four dates in July/August 2004. Independent estimates of water vapor were not available at either location.

We determined the MODIS values for comparison by choosing the pixel whose centroid was nearest the to the center

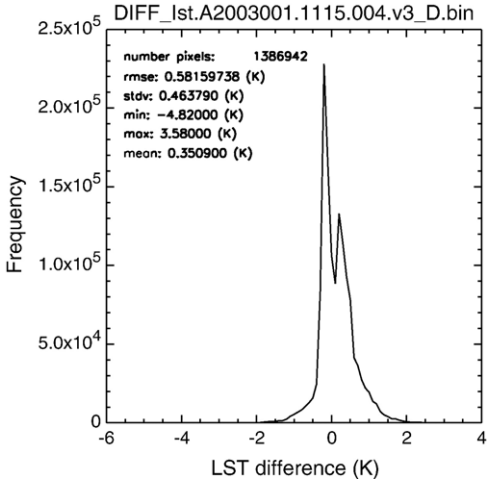

Fig. 4. LST error histogram for granule collected on January 1st, 2003 at 11:15 AM GMT.

Table 4
Validation results using Wan et al.'s (2002) field data

Site	Latitude (#) longitude (#)	Date (mm/dd/yy) time (UTC)	Water vapor			Temperature (K)			RR–MOD11 (K)	RR–in situ (K)
			TOVS	MOD07	In situ	In situ	RR	MOD11 v.004		
Mono Lake, CA	37.9712°N (37.9699°N) 119.001°W (119.007°W)	04/04/00 19:19	0.91	2.2	0.36	283.81	285.60	285.70	−0.10	1.79
Mono Lake, CA	37.9930°N (37.9924°N) 118.9646°W (−118.9700°W)	07/25/00 19:18	1.51	2.1	–	296.01	296.30	296.34	−0.04	−0.29
Mono Lake, CA	38.0105°N (38.0054°N) 118.9695°W (118.972°W)	10/06/00 19:11	1.21	1.4	0.62	290.17	290.40	290.30	0.10	+0.23
Lake Titicaca, Bolivia	16.2470°S (16.2513°S) 68.7230°W (68.7308°W)	06/15/00 15:26	1.14	1.1	0.29	285.0	285.10	285.38	−0.28	+0.10
Bridgeport, CA	38.2255°N (38.2211°N) 119.2680°W (119.272°W)	04/04/00 19:19 UTC	0.94	2.6	–	308.2	308.90	No data available	No data available	+0.70
Bridgeport, CA grassland	38.2202°N (38.2203°N) 119.2693°W (119.271°W)	07/28/00 06:09 UTC	1.55	1.6	–	281.63	281.9	282.34	−0.44	+0.27
Bridgeport, CA Grassland	38.2202°N (38.2197°N) 119.2693°W (119.263°W)	07/30/00 05:57 UTC	1.55	2.4	–	283.24	282.30	282.68	−0.38	−0.94
Rice field in California	39.5073°N (39.5062°N) 121.8107°W (121.8100°W)	07/28/00 06:10 UTC	0.93	1.4	–	291.20	292.10	292.12	−0.02	+0.90
Rice field in California	39.5073°N (39.5096°N) 121.8107°W (121.813°W)	07/30/00 05:57 UTC	0.93	3.0	–	293.02	292.70	292.70	0.00	−0.32
Bridgeport, CA Snowcover	38.2199°N (38.2149°N) 119.2683°W (119.271°W)	03/12/01 6:36 UTC	0.89	0.4	–	263.70	263.70	263.20	0.50	0.00
Average									−0.07	0.30
Standard deviation									0.28	0.73

[#] Coordinates for centroid of nearest pixel.

latitude/longitude of the test site. We ensured that the land cover type was consistent for all selected pixels. In addition to the RR product, we used values from the version 005 MODIS standard product for comparison with Wan's field data, and from the version 004 product for comparison with Coll's data in our analysis.

4.2.1. Results

The RR product compared very well with both the standard product and the field data over Wan's sites (Table 4), despite the differences between water vapor estimates from the radiosonde, the MOD07_L2 product, and the TOVS climatology. Specifically, both the MOD07_L2 and TOVS values tended to

Table 5
Validation results using Coll et al.'s (2005) field data

Site	Latitude (#) longitude (#)	Date (mm/dd/yy) time (UTC)	Water Vapor (cm)		Temperature (K)			RR–MOD11 (K)	RR–In situ (K)
			TOVS	MOD07	In situ	RR	MOD11 (v.004)		
Site #1	39.240833°N (39.2391°N) 0.297219°W (0.30211°W)	07/10/02 10:32	1.96	2.27	301.95 [a]	300.40	300.56	−0.16	−1.55
	39.240833°N (39.2365°N) 0.297219°W (0.30247°W)	07/26/02 10:32	2.07	3.20	301.25 [b, a]	299.30	299.52	−0.22	−1.95
	39.240833°N (39.2387°N) 0.297219°W (0.29084°W)	07/08/03 10:11	1.95	2.27	301.85 [c]	300.20	300.62	−0.42	−1.65
	39.240833°N (39.2415°N) 0.297219°W (0.29208°W)	07/11/03 10:42	1.96	1.35	302.05	302.20	302.3	−0.10	+0.15
	39.240833°N (39.2345°N) 0.297219°W (0.29729°W)	08/09/03 10:11	2.18	2.21	302.85 [c]	301.30	301.64	−0.34	−1.55
	39.240833°N (39.2411°N) 0.297219°W (0.29143°W)	08/12/03 10:42	2.20	1.39	304.35	303.9	304.04	−0.14	−0.45
	39.240833°N (39.2396°N) 0.297219°W (0.30083°W)	08/26/03 10:54	2.21	3.15	305.05 [b]	302.4	302.88	−0.48	−2.65
Site #2	39.250278°N (39.2417°N) 0.295244°W (0.28807°W)	07/08/04 10:24	1.95	1.82	298.45 [a]	298.5	298.46	0.04	−0.04
	39.250278°N (39.2466°N) 0.295244°W (0.29351°W)	07/27/04 10:54	2.13	1.68	301.05	301.00	301.04	−0.04	−0.05
	39.250278°N (39.2512°N) 0.295244°W (0.29594°W)	08/03/04 11:00	2.08	2.68	303.15	303.60	303.06	0.54	+0.45
	39.250278°N (39.2467°N) 0.295244°W (−0.28999°W)	08/12/04 10:54	2.28	1.89	301.85	301.60	301.60	0.00	+0.25
Average								−0.12	−0.86
Standard deviation								0.28	1.04

[#] Coordinates for centroid of nearest pixel.
Note: Cases [a,b] and [c] correspond to less ideal validation conditions.
[a] View angle >40°.
[b] Cirrus clouds.
[c] View angle >60°.

overestimate the actually water vapor amounts. The tendency for the former to overestimate actual values was noted by Wan et al. (2002). Indeed, for most dates, the MOD07_L2 value exceeded both the TOVS and radiosonde values. The mean and standard deviation of differences between the RR LST product and the standard product were −0.07 and 0.28 K, respectively. The same statistics for the RR LST product and the field data were 0.30 and 0.73 K, respectively.

Results with the Coll data set (Table 5) varied with the site, atmosphere and MODIS sampling condition. Although in situ water vapor data were not available, our comparison of the MOD07 and TOVS values again revealed differences. The mean and standard deviation of difference between the MODIS RR and standard LST products over all sites were −0.12 and 0.28 K, respectively. The same statistics for differences between the RR and field data were 0.86 and 1.04 K, respectively. Although these results are slightly poorer than those found for Wan's sites, the Coll data were measured over rice fields exclusively. This may be a particularly challenging validation type since they are irrigated with standing water. The MODIS "cropland" emissivity spectrum assumes emission from vegetation only. Further, at both sites, the MODIS values (from both the RR and standard product) were more accurate when the observations were within 40° of nadir. Such a finding is expected since high view angles have larger atmospheric path lengths and larger effective ground pixel sizes (e.g., at 40°, the pixel size is about 1.3 km × 3.2 km). Results were also more accurate on days when no cirrus clouds were observed (Coll et al., 2005).

5. Discussion

Our results suggest that, although some differences occur, the overall agreement between the MODIS standard and RR products is high with only a small bias observed at the global scale. The bias and standard deviation values appear to be mostly within, or very close to, the limit of the range of values found in the validation of the MODIS standard product. As shown in Table 4, results by Wan et al. (2002) show MODIS LST agreements with in situ measurements (for different surface types) within ±1 K. More recent validation studies by Coll et al. (2005), show a bias of +0.1 K and standard deviation of 0.6 K for comparisons of the MODIS LST against ground measurements taken over rice crop fields (see Table 5). The RR product compared very favorably with both sets of ground data as shown in Section 4.2. Still, as with the standard product, the true accuracy of the RR LST must be evaluated over time through more validation exercises against ground observation.

As noted above, in order to implement the MODIS Rapid Response System land surface temperature product, we made assumptions to avoid dependencies on other MODIS products and software toolkits. The main assumption in our approach is that a monthly, 1 by 1°, climatology for air temperature and total column water vapor is adequate to represent the spatial and temporal variability of those fields on a daily basis. Stated differently, we assumed that the LST algorithm was not especially sensitive to errors in these input fields. Obviously, LST errors increase as the deviation of the actual atmosphere from the climatology increase. Such deviations can contribute to larger precision errors despite a low overall bias error in operation. Nevertheless, by adopting this climatology, we eliminate the latency required for processing of MOD07_L2.

Note that the global analysis (Table 3) suggested that the bias, precision and uncertainty are better for the January date than for the July date. However, if we remove Antarctic from the global analysis, the results are better in July rather than January. This likely results from systematic differences in atmospheric parameters as retrieved by MODIS and estimated by our climatology over the South Pole. Further analysis of these differences was outside of the scope of this study.

Several limitations have been identified in the MODIS LST standard product that equally apply to the LST RR product. These include the unknown accuracy of the landcover based emissivity values used in the retrieval of the surface temperature. Despite the efforts to develop and validate emissivity fields globally, there remains much uncertainty in published values. Studies (Wan et al., 2002) suggest that the classification-based emissivities used in the split-window algorithm are too high, especially in the semi-arid and arid regions. Wan et al. (2002) recommend that the 1-km LST product retrieved by the spit-window be used for lakes, snow/ice, and dense vegetation, for which the uncertainty in emissivity is lower. Estimates of LST over bare and sparse vegetation areas may be more accurate from other products in the MODIS LST product suite.

The fact that the standard LST relies on a static landcover map suggests that some of the dynamic character of the emissivity, observed in the field and in the lab, may not be accounted for in the LST retrievals. To account for some of these dynamic characteristics, the standard product adopts distinct values of emissivity for senescent and green vegetation which should create some seasonal variability in the retrievals. Note that this capability is currently not implemented in the RR system, i.e., only "green" emissivity values are used. This can justify some of the differences observed in the comparison of the products. For example, for a woody savanna surface at kinetic temperature at 300 K, the differences in senescent and green emissivity values would lead to changes in brightness temperature in channel 31 of 1 K (from 299 for green conditions to 298 for senescent conditions). Similar values are found for band 32. The differentiation of green and senescent conditions will be implemented in the RR system in the future to address these possible differences.

The no-cloud-screening approach chosen by the RR system is an advantage for a number of applications. Because the MOD35_L2/MYD35_L2 product often overestimates cloudiness (e.g., over deserts), the standard LST product often shows a fill value in valid cloud-free conditions. On the contrary, the RR LST product is calculated for every valid pixel. A cloud mask can be applied afterwards if necessary.

In our future work, we plan to address several other sources of uncertainty, including sun-view geometry effects, within-class emissivity variability, cloud masking and the climatology of water vapor and surface air temperature. For example, Pinheiro et al. (2004b) recently demonstrated that split window

LST products are sensitive to the sun-view geometry at the time of observations, particularly when viewing structured canopies where both shadowed and sunlit components are visible. The geometry differences can lead to significant differences in the retrieved LST. Similarly, Pinheiro et al. (2006) recently developed a "continuous fields" approach to surface emissivity based on the MODIS fractional cover product. We also plan to explore simple cloud detection algorithms such that a cloud mask could be incorporated into the product's QA fields. Finally, a straightforward improvement in the current RR algorithm may be possible through the replacement of TOVS climatology with NOAA's National Centers for Environmental Prediction (NCEP) model forecasts.

Although the RR product deviates some from the standard product, it should nevertheless be valuable to many users due to its timeliness. It facilitates monitoring, in near-real time, of surface energy conditions around the globe, potentially allowing for timely interventions in some applications. Users may include those interested in monitoring crop conditions, irrigation scheduling, forest fire fuel condition, fire risk, and agricultural and hydrological drought or heat indices, or polar icebergs. Indeed, in the first quarter of 2006, approximately 500 different users have downloaded nearly 3000 LST files per month.

A large number of users use the RR System because of its additional ability to meet user specific requirements as the RR System allows for customized subsetting and compositing of data. For example, the RR System is currently subsetting and archiving daily LST data for the state of New Mexico for studies aiming to improve the estimates of evapotranspiration over the area, and evaluation of the product within a land surface model assimilation system (Pinheiro et al., 2004a).

6. Conclusions

We modified the standard MODIS land surface temperature (LST) processing algorithm, used to generate product MOD11_L2/MYD11_L2, as needed for implementation within the MODIS Rapid Response (RR) System. To achieve near-real time retrievals of this variable we removed dependencies on external products that would create latency in product generation. Specifically, we adopted a $1°\times1°$ TOVS climatology for air temperature and water vapor to substitute the equivalent MODIS variables from MOD07_L2. Minor modifications were also made in the estimation of top-of-atmosphere brightness temperature and land emissivity determination. Comparisons of the new product against the standard MODIS LST product show that this is a reasonable assumption and that, for most cases, the biases created by this method are small (<0.1 K) for most granules studied, and are, in general, within the accuracy to MODIS standard product itself. Comparisons against field data from sites in Europe and North America suggest the absolute uncertainty is less than 1 K — approximately the same uncertainty attributed to the standard LST product. Comparisons against the MODIS LST standard product suggest the RR LST tends to be slightly higher (biases<0.1 K) and that product differences are lowest for daytime data (versus nighttime data). These differences are more pronounced around the Equator than at mid latitudes.

The new code allows for a stand-alone processing algorithm for retrievals of MODIS land surface temperature fields and can be implemented in Direct Broadcast or similar systems. This capability is relevant for any user community that requires MODIS LST within a few hours of satellite overpass. All RR software system is written in C code and is available at no cost to any user.

Acknowledgements

The authors would like to thank Dr. Z. Wan for his help with the official's MODIS LST code, Louis Giglio with suggestions for MODIS brightness temperature determination, Jack Xiong for information on MODIS sensor characteristics, and Nazmi Saleous and Robert Wolfe for guidance on MODAPS processing system. We are also grateful to Chris Justice who provided overall leadership of the Rapid Response project.

Appendix A. Time-of-day Corrections to TOVS Water Vapor and Surface Air Temperature Climatologies

The HIRS2/MSU sensors, collectively referred to as TOVS (TIROS Operational Vertical Sounder) have flown on the NOAA Operational Polar Orbiting Satellites TIROS-N, NOAA 6-8, NOAA 8-14, from November l978 to May 2005. The data has been analyzed using a frozen processing methodology (Susskind et al., 1997) to produce 2–4 times daily global fields of land/ocean surface skin temperature, atmospheric temperature and moisture profile, cloud height and fractional cloud cover, outgoing longwave radiation (OLR) and Clear Sky OLR, and precipitation, on a $1°\times1°$ latitude–longitude grid. This TOVS Pathfinder Path A data set covers the period December 1978–May 2005.

To correct for orbital drift effects in the TOVS patforms, a methodology has been developed to account for differences in the retrieved geophysical parameters due to differences in the TOVS sampling time. This allows for one to adjust geophysical parameters determined at any time of day to what they would have been if observed at another time of day.

The panels in Fig. A.1 indicate the magnitude of the orbital effect. Fig. A.1a shows the local equatorial crossing time of the different satellites as a function of time. NOAA 6, NOAA 9, NOAA 10 and NOAA 12 are referred to as "morning" satellites, with a relatively stable orbit roughly at 7:30 AM/PM local time. TIROS N, NOAA 7, NOAA 9, 11, and 14 are "afternoon" satellites with nominally 1:30 AM/PM equator crossing times. The afternoon orbits drift quickly to later in the day with time past launch. Most dates in the multi-decadal record are sampled by two satellites (four times a day), although some gaps exist due to satellite or instrument malfunctions.

Fig. A.1b shows monthly global mean values of surface air temperature for all times of day measured. To develop a single standard time series from the different sampling times, the observations in a month and year, $T_{M,Y}$ at time $Z_{M,Y}$, are

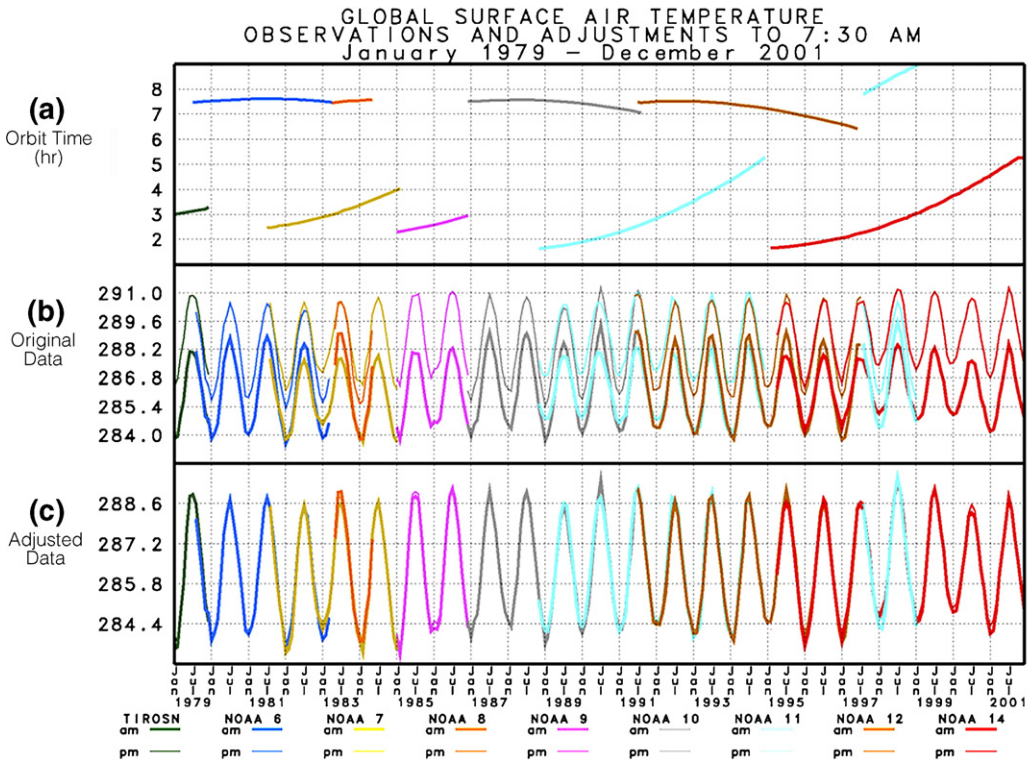

Fig. A.1. TOVS global surface air temperature observations and adjustments (see text for explanation).

corrected to what they would have been if all were made at a constant local time, arbitrarily set to 7:30 AM, according to

$$T'_{\mathrm{M,Y}}(7:30) = T_{\mathrm{M,Y}}(Z_{\mathrm{M,Y}}) - \delta T_{\mathrm{M}}(Z_{\mathrm{M,Y}}). \quad (1)$$

The correction is modeled as a function of the time of year the time-of-day

$$\delta T_M(Z_{M,Y}) = G(M)F(Z_{\mathrm{M,Y}} - 7:30) = G(M)F(\Delta Z). \quad (2)$$

$G(M)$ is taken as periodic in 6 months

$$G(M) = A + B\cos\left(\frac{M\pi}{6}\right) + C\sin\left(\frac{M\pi}{6}\right) + D\cos\left(\frac{M\pi}{3}\right) + E\sin\left(\frac{M\pi}{3}\right) \quad (3)$$

while is periodic in 6 h

$$F(\Delta Z) = 1 + \sum_{n=1,4} A_n \cos\left(\frac{n\pi\Delta Z}{12}\right) + \sum_{n=1,4} B_n \sin\left(\frac{n\pi\Delta Z}{12}\right) \quad (4)$$

giving a total of 40 unknown coefficients. Differences between the monthly mean observations for each month, taken at all times of day, are used to construct multilinear equations to solve for these coefficients. Separate coefficients are found for each $5° \times 5°$ latitude–longitude bin. These corrections are subsequently smoothed in space and applied to retrieved standardized geophysical parameters (e.g., surface air temperature as needed for the present study) on a $1° \times 1°$ latitude–longitude bin. Note that the corrections depend only on time of day and not on satellite. Soundings can be corrected to any common local time, Z_0 using Eqs. (1)–(4), and setting ΔZ to be $(Z_{\mathrm{M,Y}} - Z_0)$.

Fig. A.1c shows the global mean values of the corrected air temperature data at 7:30 AM. The satellite independent time of day correction works extremely well for all satellites and time periods. Similar adjustments have been made for temperatures at all vertical levels of atmosphere, as well as all other products derived in the Pathfinder data set, including total precipitable water above the surface. The 25-year monthly mean climatologies for surface air temperature and total precipitable water above the surface are the two fields used in conjunction with the analysis of the MODIS data in the present study.

References

Coll, C., Caselles, V., Galve, J., Valor, E., Niclos, R., Sanchez, J., et al. (2005). Ground measurements for the validation of land surface temperatures derived from AATSR and MODIS data. *Remote Sensing of Environment*, *97*, 288–300.

Guenther, B., Xiong, X., Salomonson, V. V., Barnes, W. L., & Young, J. (2002). On-orbit performance of the Earth Observing System Moderate Resolution Imaging Spectroradiometer; first year of data. *Remote Sensing Environment*, *83*(1-2), 16–30.

Justice, C. O., Townshend, J. R. G., Vermote, E. F., Masuoka, E., Wolfe, R. E., Saleous, N., et al. (2002). An overview of MODIS land data processing and product status. *Remote Sensing of Environment*, *83*, 3–15.

Pinheiro, A. C., Arsenault, K., Houser, P., Toll, D., Kumar, S., Matthews, D., et al. (2004a). Improved evapotranspiration estimates to aid water management practices in the Rio Grande Basin. *Proceedigns of IGARSS04, Anchorage, Alaska, September.*

Pinheiro, A. C. T., Mahoney, R., Privette, J. L., & Tucker, C. J. (2006). A daily long term record of NOAA-14 AVHRR land surface temperature over Africa. *Remote Sensing of Environment*, *103*(2), 153−164.

Pinheiro, A. C. T., Privette, J. L., Mahoney, R., & Tucker, C. J. (2004b). Directional effects in a daily AVHRR land surface temperature dataset over Africa. *IEEE Transactions on Geosciences Remote Sensing*, *42*(9), 1941−1954.

Sohlberg, R., Descloitres, J., & Bobbe, T. (2001, September/October). MODIS land rapid response: Operational use of terra data for USFS wildfire management. *The Earth Observer*, *13*(5), 8−14.

Susskind, J., Piraino, P., Rokke, L., Iredell, L., & Mehta, A. (1997). Characteristics of the TOVS pathfinder path A dataset. *Bulletin of the American Meteorological Society*, *78*, 1449−1472.

Wan, Z., & Dozier, J. (1996). A generalized split-window algorithm for retrieving land-surface temperature from space. *IEEE Transactions on Geoscience and Remote Sensing*, *34*, 892−905.

Wan, Z., Zhang, Y., Zhang, Q., & Li, Z. -L. (2002). Validation of the land surface temperature products retrieved from the Terra Moderate Resolution Imaging Spectroradiometer data. *Remote Sensing of Environment*, *83*, 163−180.